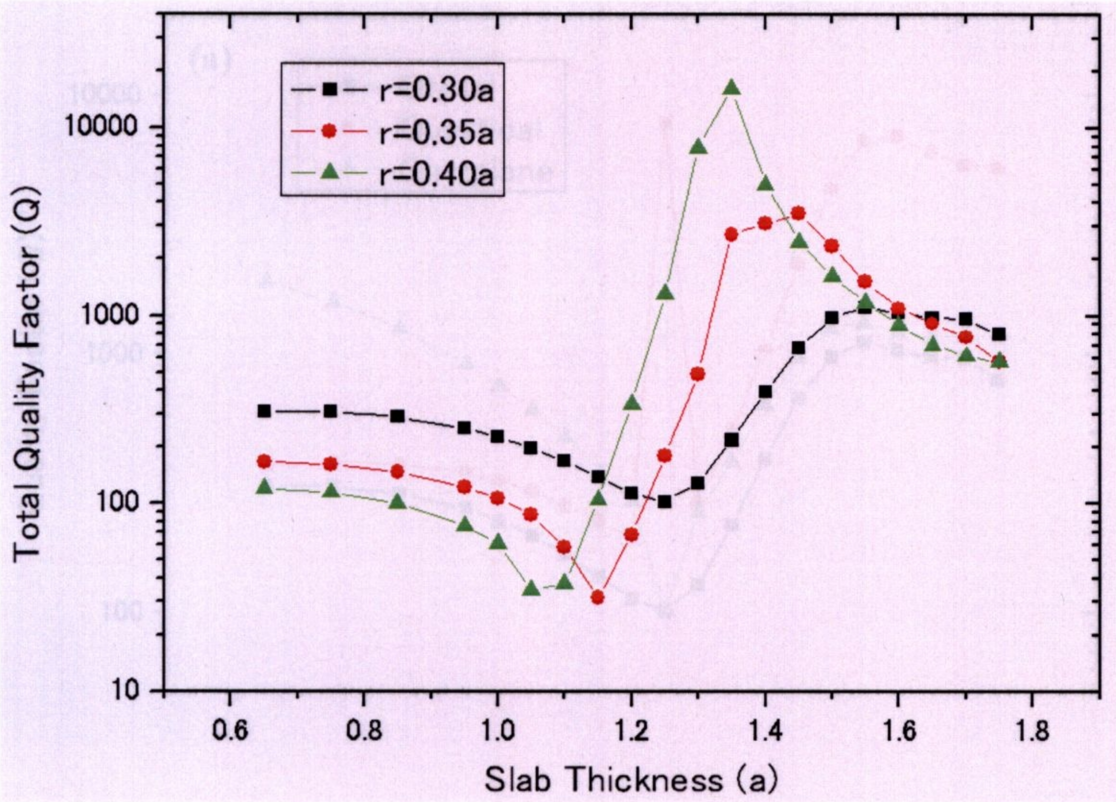

Figure 4.3 Dependence of total *Q*-factor on slab thickness for the dipole mode of the H1-defect cavity with r = 0.30a (square), r = 0.35a (circle), and r = 0.40a (triangle)

4.4 Results Analysis

In this section, the results shown in last section will be discussed. From Fig. 4.3, the total *Q*-factors of all structures are only few hundreds or less than a hundred in the thin slab region. These results are corresponding to the values of the *Q*-factor of conventional dipole modes as already mentioned above. So as to understand the mechanism of higher total *Q*-factor of the structure with r = 0.30a than those of the structures with r = 0.35a and 0.40a and the mechanism of the drop of *Q*-factor as the slab thickness increases, the total *Q*-factor of each structure was separated into vertical and in-plane components and shown in Fig. 4.4 for the all structures. In each plot, the total *Q*-factor is limited by the vertical *Q*-factors in the thin slab region. The vertical *Q*-factor is low due to the degeneracy of the dipole mode and is enhanced when the radius of air holes is reduced because the cavity size is bigger, and also the defect mode frequency is lower, where the radiation loss is less. The relation between the defect mode frequency and the slab thickness of each structure is shown in Fig. 4.5. The dependence of the mode frequency on the slab thickness is originated from

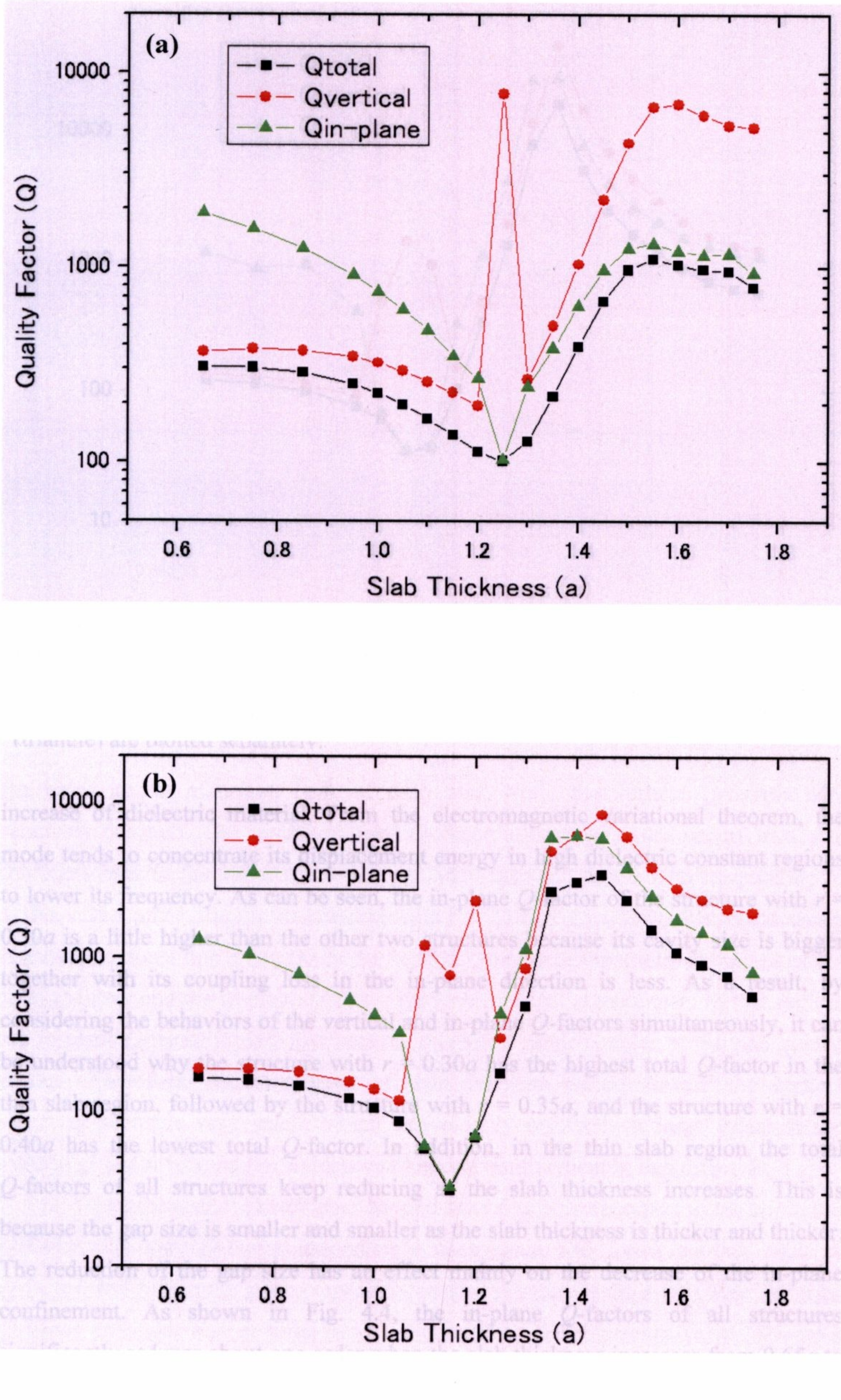
(a)
Qtotal
Qvertical
Qin-plane
Quality Factor (Q)
10000
1000
100
10
0.6
0.8
1.0
1.2
1.4
1.6
1.8
Slab Thickness (a)
(b)
Qtotal
Qvertical
Qin-plane
Quality Factor (Q)
10000
1000
100
10
0.6
0.8
1.0
1.2
1.4
1.6
1.8
Slab Thickness (a)

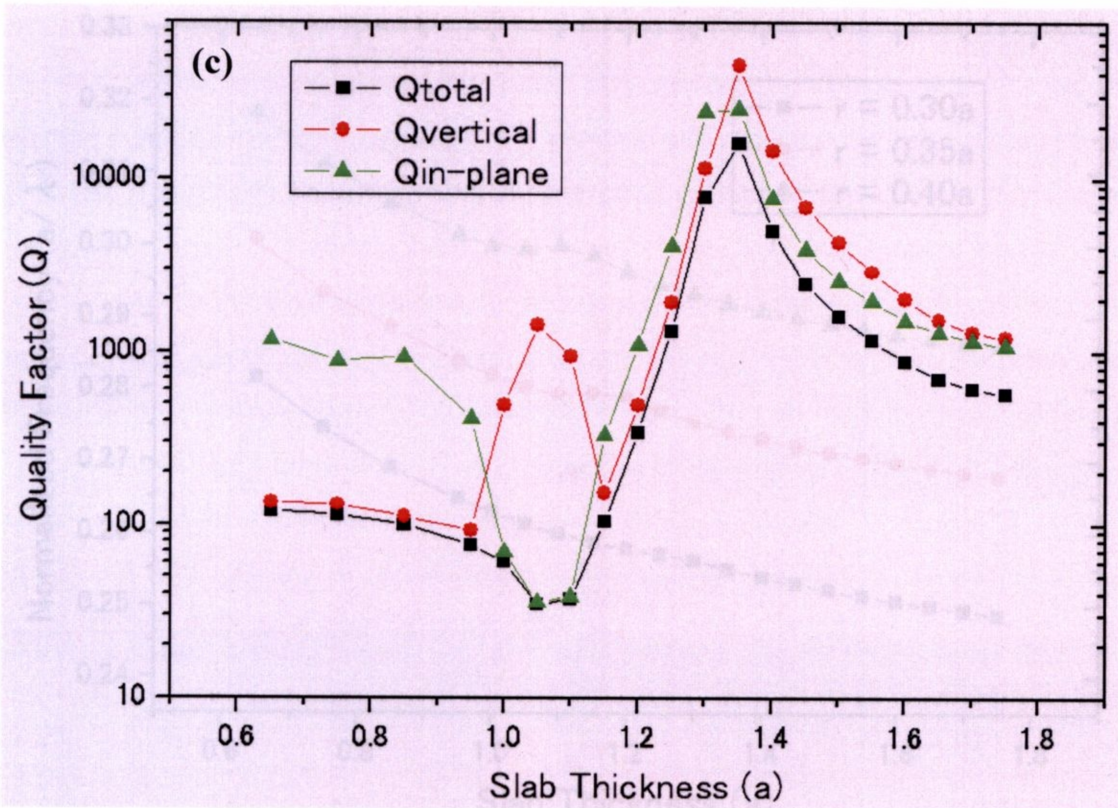

Figure 4.4 Dependence of *Q*-factor on slab thickness for the dipole mode of the H1-defect cavity with (a) $r = 0.30a$, (b) $r = 0.35a$, and (c) $r = 0.40a$. In addition to the total Q-factor (square), the vertical Q-factor (circle) and the in-plane *Q*-factor (triangle) are plotted separately.

increase of dielectric material. From the electromagnetic variational theorem, the mode tends to concentrate its displacement energy in high dielectric constant regions to lower its frequency. As can be seen, the in-plane *Q*-factor of the structure with $r = 0.30a$ is a little higher than the other two structures because its cavity size is bigger together with its coupling loss in the in-plane direction is less. As a result, by considering the behaviors of the vertical and in-plane *Q*-factors simultaneously, it can be understood why the structure with $r = 0.30a$ has the highest total *Q*-factor in the thin slab region, followed by the structure with $r = 0.35a$, and the structure with $r = 0.40a$ has the lowest total *Q*-factor. In addition, in the thin slab region the total *Q*-factors of all structures keep reducing as the slab thickness increases. This is because the gap size is smaller and smaller as the slab thickness is thicker and thicker. The reduction of the gap size has an effect mainly on the decrease of the in-plane confinement. As shown in Fig. 4.4, the in-plane *Q*-factors of all structures significantly reduces about one order when the slab thickness increases from $0.65a$ to

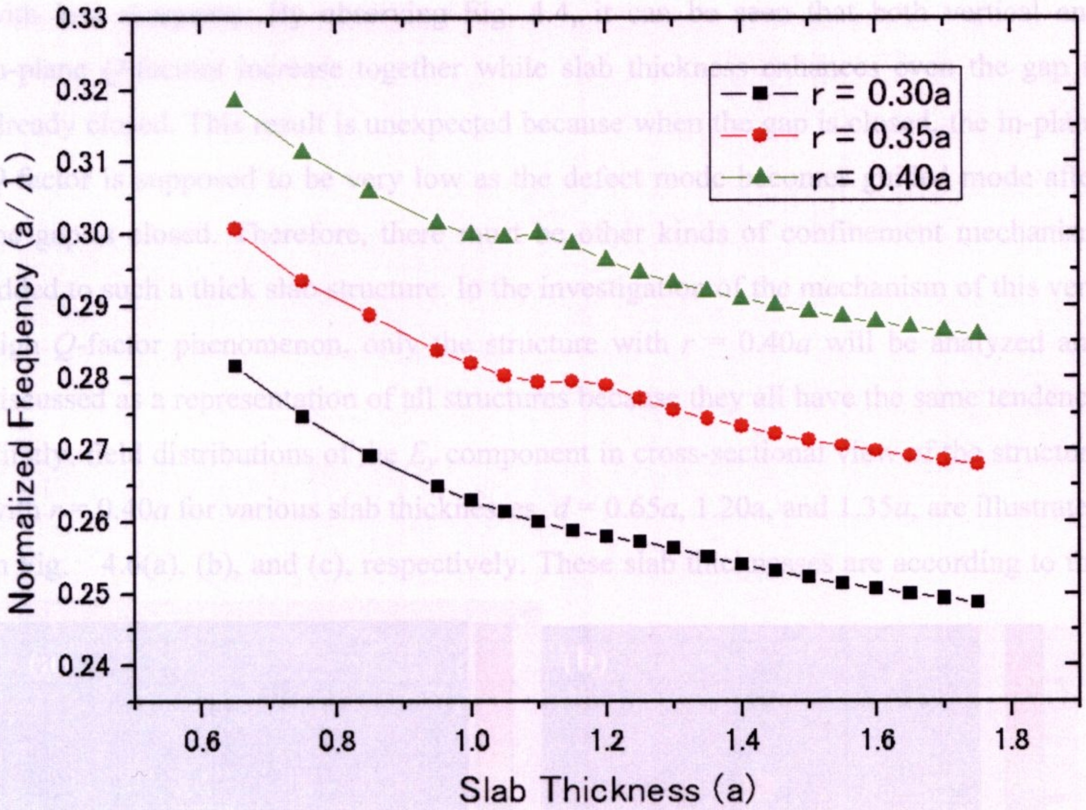

Figure 4.5 Dependence of the mode frequency on the slab thickness for the structures with $r = 0.30a$ (square), $r = 0.35a$ (circle), and $r = 0.40a$ (triangle).

the value at the minimum peak of each plot, while the vertical *Q*-factors stay relatively constant. The minimum total *Q*-factor of each structure occurs at a slab thickness near to the value where the gap starts closing, which is corresponding to 1.10*a*, 1.25*a*, and 1.20*a* for the structure with $r = 0.30a$, 0.35*a*, and 0.40*a*, respectively. It should be noted that the peaks of the vertical *Q*-factor at the minimum values of the total *Q*-factor and the in-plane *Q*-factor have no physical significance. In that region, the in-plane *Q*-factor is very low because the defect mode couples to the slab guided mode. Therefore, the component of light that can radiate toward the vertical direction becomes very small, which unavoidably results in a large value of the vertical *Q*-factor without any evidences of strong confinement in that direction.

When the slab thickness goes beyond the value corresponding to the minimum *Q*-factor, the total *Q*-factor immediately rises again and forms another peak of *Q*-factor, the maximum peak, especially in the structure with $r = 0.40a$, the total *Q*-factor enhances almost three orders compared to the minimum value. The total *Q*-factor of the structures with $r = 0.30a$ and 0.35*a* also have peaks of *Q*-factor but with less sharpness. By observing Fig. 4.4, it can be seen that both vertical and in-plane Q-factors increase together while slab thickness enhances even the gap is already closed. This result is unexpected because when the gap is closed, the in-plane Q-factor is supposed to be very low as the defect mode becomes guided mode after the gap is closed. Therefore, there must be other kinds of confinement mechanism added to such a thick slab structure. In the investigation of the mechanism of this very high Q-factor phenomenon, only the structure with $r = 0.40a$ will be analyzed and discussed as a representation of all structures because they all have the same tendency. Firstly, field distributions of the E_y component in cross-sectional view of the structure with $r = 0.40a$ for various slab thicknesses, $d = 0.65a$, 1.20a, and $1.35a$, are illustrated in Fig. 4.6(a), (b), and (c), respectively. These slab thicknesses are according to the

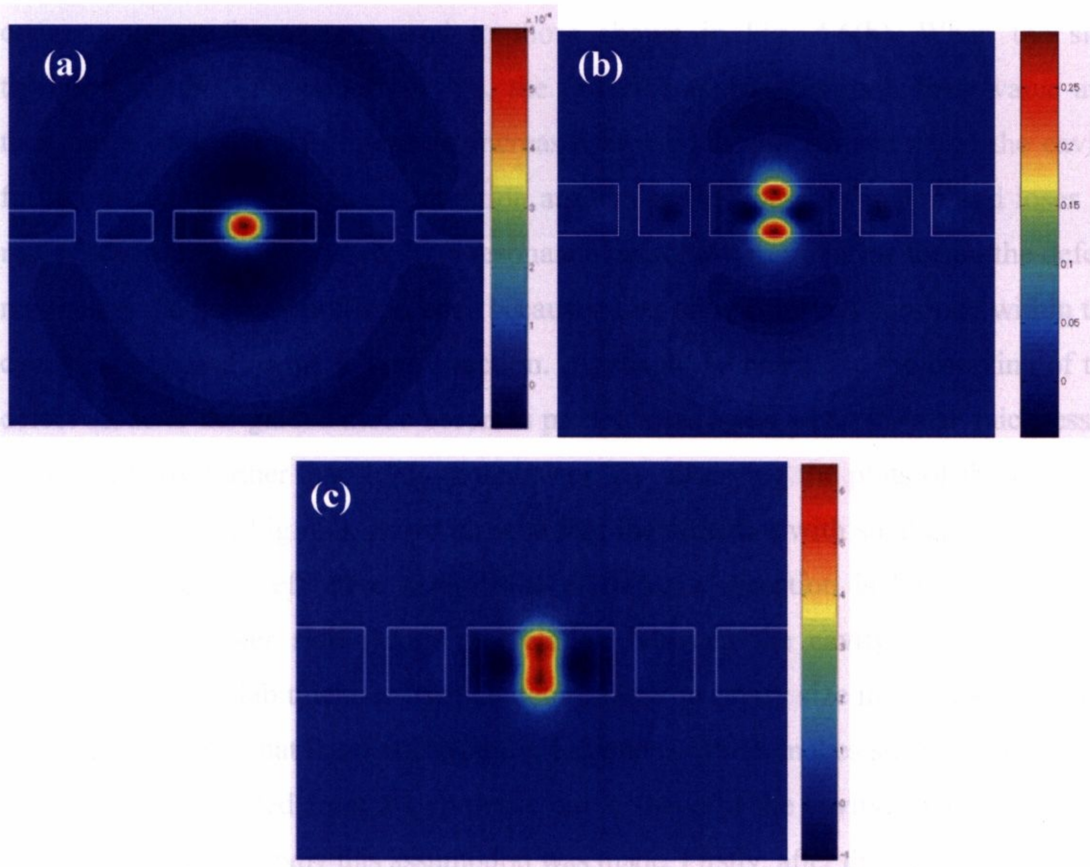

Figure 4.6 Field distributions of E_y component of the dipole mode viewed in cross-section of the slab along $\Gamma - M$ for the structures with (a) $d = 0.65a$, (b) $d = 1.20a$, and (c) $d = 1.35a$. The lines shown in the figures indicate the boundaries of the slab with air holes.

thicknesses where the gap is still open, the gap starts closing, and the Q-factor is the highest, respectively. The solid lines shown in the figures indicate boundaries of the slabs with air holes. According to Fig. 4.6(a), in the structure with $d = 0.65a$, in which the defect mode frequency is located in the gap, the E_y-field of the dipole mode is well confined within the slab and its maximum locates at the center of the slab. However, when the slab becomes so thick that the gap is closed, antinode of the field splits into two components corresponding to the coupling of the defect mode to the second-order guided mode of the slab. These splitting peaks are shifted to the positions near the surface of the slab as shown in Fig. 4.6(b). The splitting of peaks is corresponding to the field distribution of the second-order guided mode, which comes down toward the lowest-order band and finally overlaps with the defect mode frequency. As a result, the Q-factor at this slab thickness is very low, that is, the defect mode can be guided through the slab. However, as shown in Fig. 4.6(c), when the slab thickness is kept increasing, the splitting peaks come closer to each other and their overlapping components are larger compared to those shown in Fig. 4.6(b). When the slab thickness reaches the value of 1.35a, the Q-factor approaches its highest value and then drops after the slab thickness increases beyond $1.35a$. It means that the cavity fulfills the additional resonant condition at the slab thickness $d = 1.35a$ and loses its resonance after that. Moreover, this resonance must have more influence on the defect mode than the guided condition does because most of light is well confined within the cavity, not guided to the lateral direction. . It should be noted that the coupling of the defect mode to the guided mode becomes predominant again when the slab thickness is increased fairly further than 1.75a (not shown). By observing the plots of the Q-factor of all structures in Fig. 4.3, it can be seen that the structure with smaller radius of air holes, in which its effective cavity size in in-plane direction is larger, attains its resonance at thicker slab. From the relation between the cavity size in in-plane direction and the slab thickness, which determines the cavity size in vertical direction; it may be assumed that the confinement mechanism, which makes such a kind of high Q cavity, is originated from a symmetric cubic shape of the cavity. In addition, there are two more reasons why this assumption was made. Firstly, after the gap is closed, both $Q_{//}$ and $Q_{\perp}$ change in the same trend, which means that the additional confinement mechanism affects all three dimensions of the cavity. Secondly, this additional confinement mechanism cannot be observed in any thicker slab regions than that shown in Fig. 4.3.

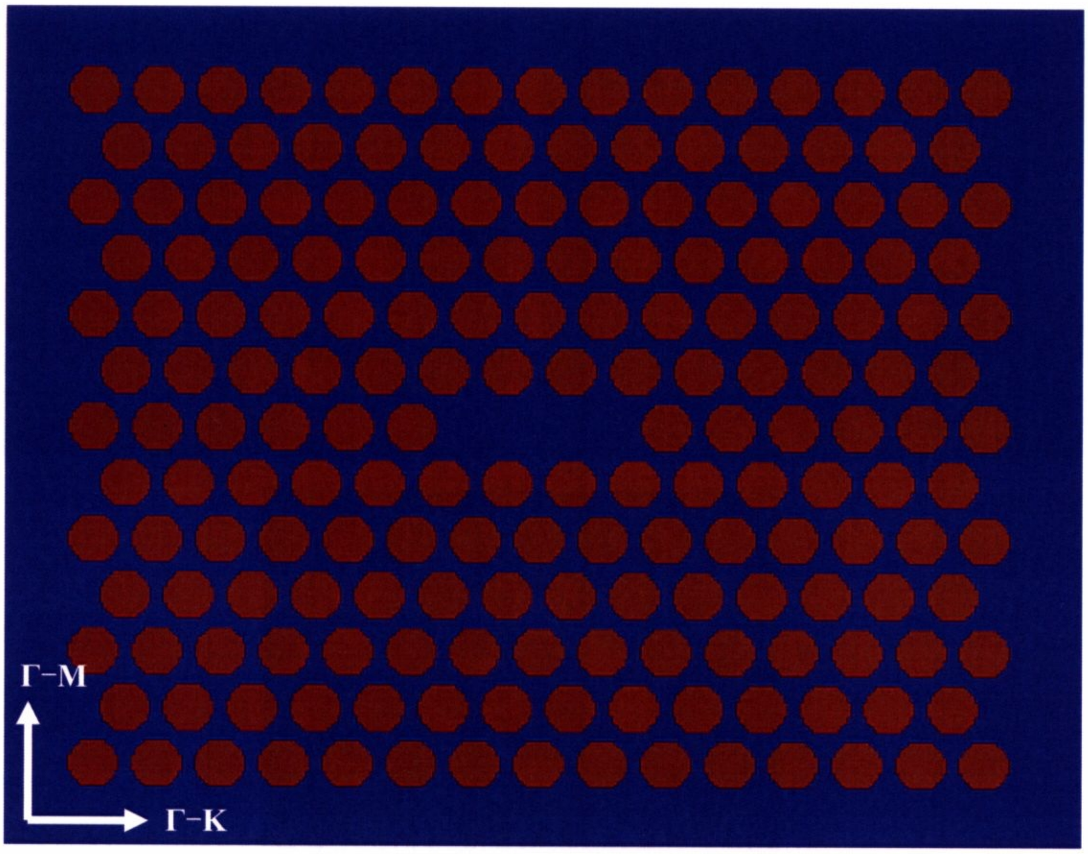

Figure 4.8 Schematic of the L3-defect slab nanocavity with three missing air holes.

In order to confirm the assumption of this kind of confinement mechanism, another type of defect cavity was also applied to an air-bridge slab structure for comparison. A three-missing-hole (L3) type, in which three air holes in $\Gamma - K$ direction are removed, was considered. The L3-defect cavity is very appropriate to be adopted as a comparator, because it has an asymmetric shape, which is long in one side. The model of the L3-defect cavity is shown in Fig. 4.8. In the calculation of L3-defect structure, few periods of air holes were added to the calculation model to avoid a lack of air holes surrounding the cavity, which will lead to excessive lateral scattering losses; then, the comparison with the results of H1-defect cavity cannot be performed properly. A fundamental mode of the L3-defect cavity is exploited in the calculation as a defect mode. It is a proper choice to use the fundamental mode of L3-defect cavity to compare with the dipole mode of H1-defect cavity, because their field distributions are much alike to each other as shown in Fig. 4.9. Field distribution of the E_y component of the fundamental mode has an antinode at the center of the cavity like that of the dipole mode of the H1-defect cavity.

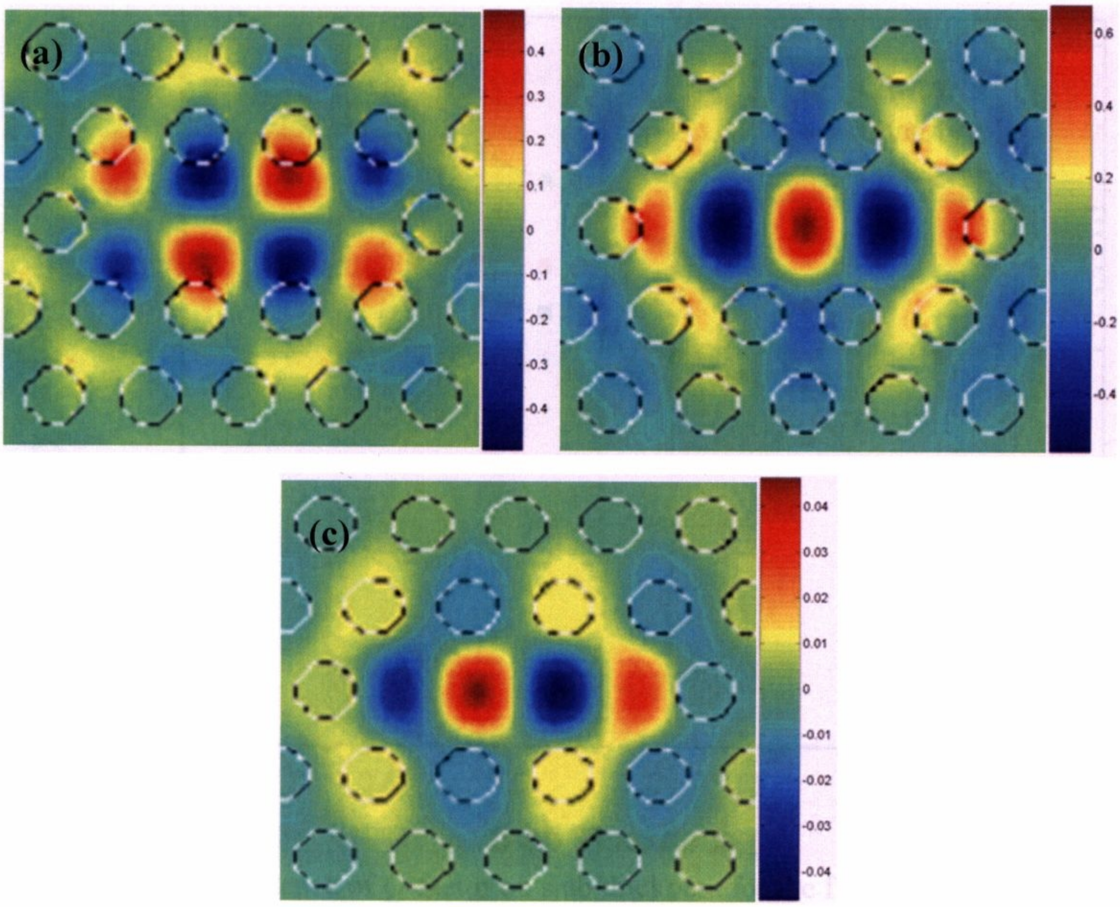

Figure 4.9 Field distributions of the fundamental mode of the L3-defect structure detected at the center of the slab (a) E_x component, (b) E_y component, and (c) H_z component. The circular dotted lines show the regions of air holes for reference.

The dependence of the Q-factor on slab thickness of the L3-defect structure is shown in Fig. 4.10. The radius of air holes was set to be equal to 0.30*a*, not 0.40*a* like in the case of the H1-defect cavity, because the L3-defect structure with $r = 0.40a$ was not suitable to be used as the comparator due to its fundamental mode embedded in the first band. According to Fig. 4.10, the total Q-factor is highest at the slab thickness around 0.65a, and decreases as the slab thickness increases beyond the value at the maximum Q-factor due to decreasing in gap size. It can be seen that no peak of the total Q-factor is observed in the range of slab thickness after the gap is closed. That is, when the gap is already closed, the defect mode is coupled to the second-order guided mode, which has frequency equivalent to its. The cross-sectional field profiles of the mode before and after the gap is closed are shown in Fig. 4.11(a) and (b), respectively. Unfortunately, unlike the H1-defect structure, the L3-defect cavity does not have

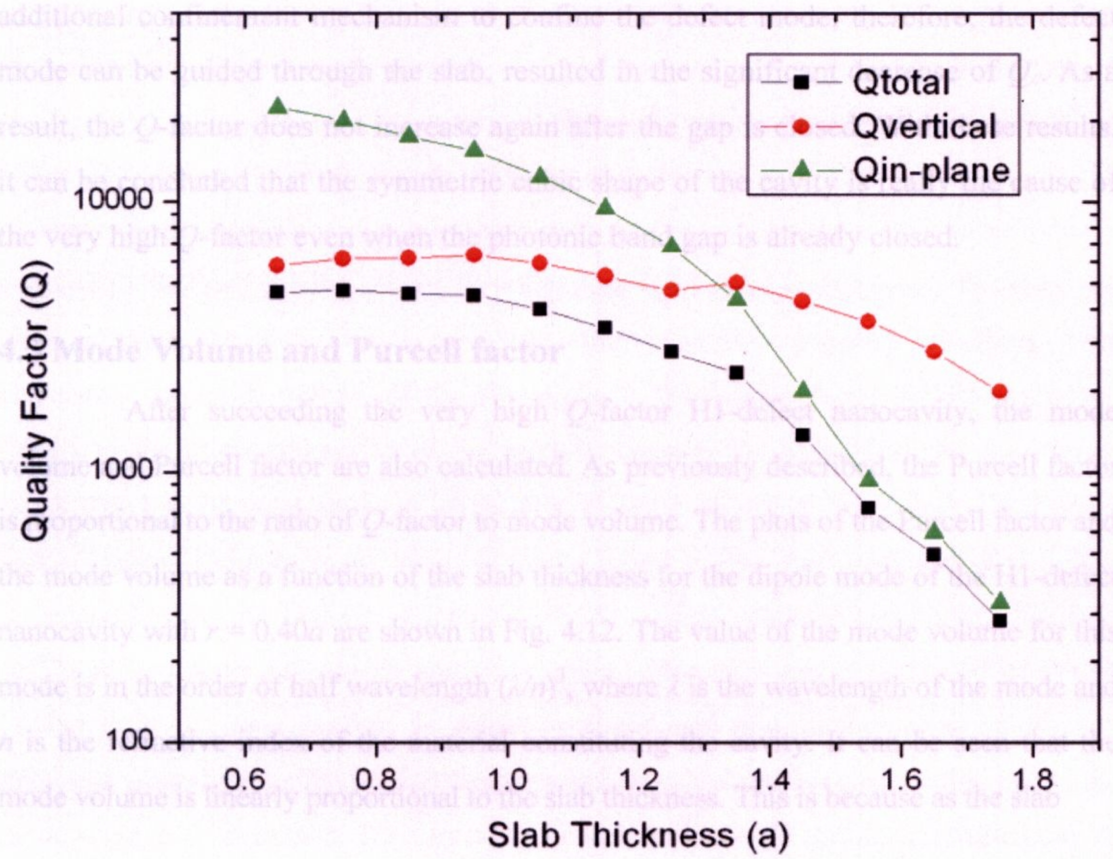

Figure 4.10 Dependence of Q-factor on slab thickness for the fundamental mode of the L3-defect cavity with $r = 0.30a$. In addition to the total Q-factor (square), the vertical Q-factor (circle) and the in-plane Q-factor (triangle) are plotted separately.

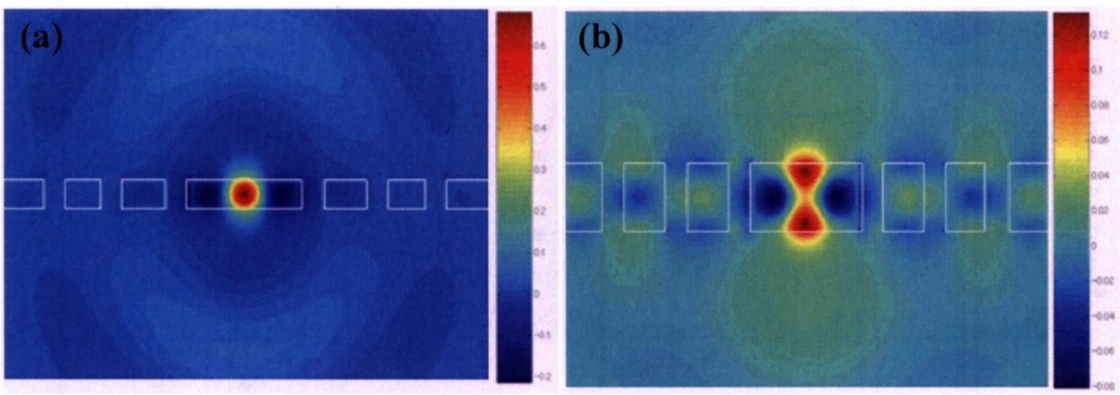

Figure 4.11 Field distributions of E_y component of the fundamental mode viewed in cross-section of the slab along $\Gamma - M$ for the structures with (a) $d = 0.65a$, and (b) $d = 1.55a$. The lines shown in the figures indicate the boundaries of the slab with air holes.

additional confinement mechanism to confine the defect mode; therefore, the defect mode can be guided through the slab, resulted in the significant decrease of $Q_{//}$. As a result, the Q-factor does not increase again after the gap is closed. With these results, it can be concluded that the symmetric cubic shape of the cavity is really the cause of the very high Q-factor even when the photonic band gap is already closed.

4.5 Mode Volume and Purcell factor

After succeeding the very high Q-factor H1-defect nanocavity, the mode volume and Purcell factor are also calculated. As previously described, the Purcell factor is proportional to the ratio of Q-factor to mode volume. The plots of the Purcell factor and the mode volume as a function of the slab thickness for the dipole mode of the H1-defect nanocavity with $r = 0.40a$ are shown in Fig. 4.12. The value of the mode volume for this mode is in the order of half wavelength $(\lambda/n)^3$, where λ is the wavelength of the mode and n is the refractive index of the material constituting the cavity. It can be seen that the mode volume is linearly proportional to the slab thickness. This is because as the slab

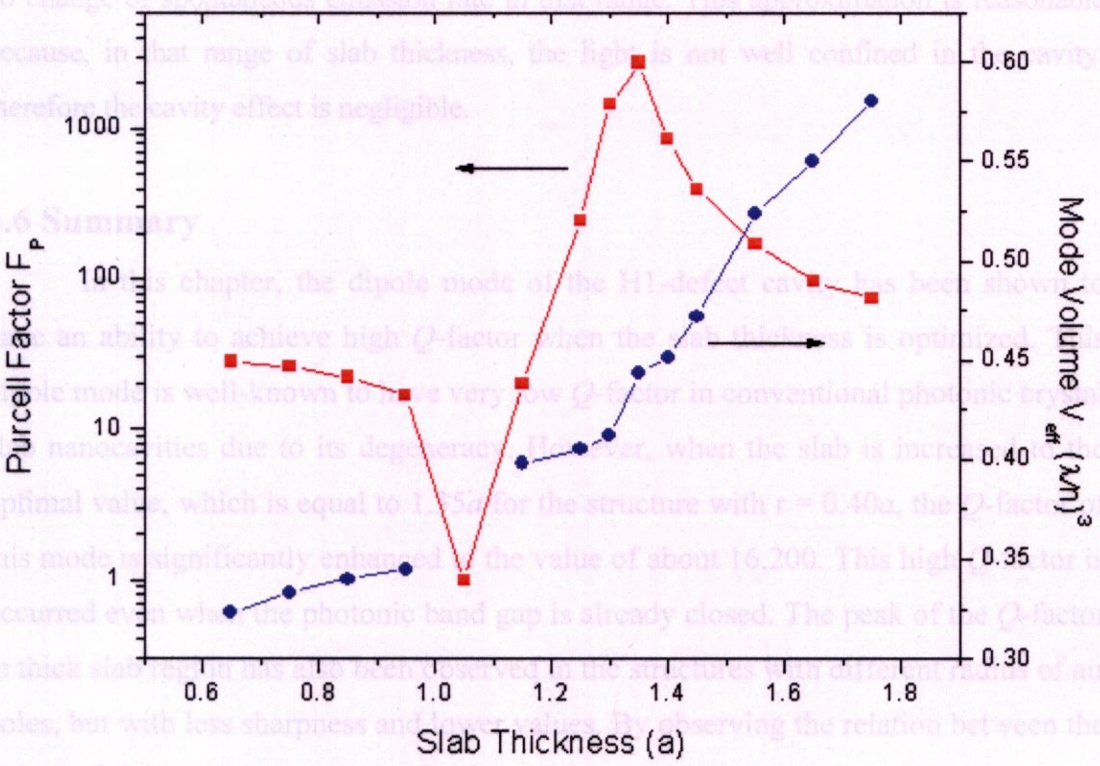

Figure 4.12 Mode volume and Purcell factor for the dipole mode of the H1-defect cavity with $r = 0.40a$.

becomes thicker and thicker, the size of the cavity becomes larger and larger. As a result, the volume of confined mode increases due to the cavity size. It should be noted that, as can be seen in the plot, the plot of mode volume is missing at the slab thickness about $1.00a$. That value of slab thickness corresponds to the value of slab thickness with the minimum peak of Q-factor shown in Fig. 4.4(c). At that slab thickness, the defect mode is coupled to the slab guided mode; therefore, the light is guided through the slab, not confined inside the cavity. Hence the mode volume cannot be properly calculated. After calculating the mode volume of the dipole mode, the Purcell factor is then evaluated. Owing to the linear proportion of the mode volume to the slab thickness, the Purcell factor then has the same tendency as the total Q-factor shown in Fig. 4.4(c). The Purcell factor reaches the maximum value of about 2,800 at the slab thickness $d = 1.35a$, corresponding to the highest Q structure. Such a high value of the Purcell factor is sufficient for realizing the cavity with the coupling efficiency very closed to 100% as will be shown in the next chapter. It should be mentioned that, at the range of the slab thickness around $1.00a$, the Purcell factor cannot be calculated because, in that range, the mode volume is undefined. Therefore it is approximated to be about 1 corresponding to no change of spontaneous emission rate in that range. This approximation is reasonable because, in that range of slab thickness, the light is not well confined in the cavity, therefore the cavity effect is negligible.

4.6 Summary

In this chapter, the dipole mode of the H1-defect cavity has been shown to have an ability to achieve high Q-factor when the slab thickness is optimized. This dipole mode is well-known to have very low Q-factor in conventional photonic crystal slab nanocavities due to its degeneracy. However, when the slab is increased to the optimal value, which is equal to $1.35a$ for the structure with $r = 0.40a$, the Q-factor of this mode is significantly enhanced to the value of about 16,200. This high Q-factor is occurred even when the photonic band gap is already closed. The peak of the Q-factor in thick slab region has also been observed in the structures with different radius of air holes, but with less sharpness and lower values. By observing the relation between the values of slab thickness at the peak of the Q-factor and the in-plane cavity size of each structure with various radii of air holes, the mechanism of the high Q-factor value of this mode has been investigated and assumed to be the symmetric cubic shape of the cavity. This assumption has been proven by comparing the results with the L3-defect cavity, in which the cubic shape is asymmetric. The Q-factor of the fundamental mode of the L3-defect cavity abruptly drops after the gap is closed and does not considerably increases again even varying the slab thickness in wide range. As a result, it has been confirmed that the symmetric cubic shape of the cavity is really the cause of the very high Q-factor of the dipole mode even when the photonic band gap is already closed. Finally, the mode volume and the Purcell factor of the dipole mode of the designed cavity have been calculated and shown as the function of the slab thickness. The mode volume of this mode is in the order of half wavelength. The large Purcell factor of 2,800 has been achieved in the structure with $r = 0.40a$ and $d = 1.35a$. Such a large Purcell factor is promising for obtaining the cavity with coupling efficiency of about 100% as will be discussed in the next chapter.